

# Calculation of Electron Drift Mobility at Low Electric Field in $\text{Hg}_{1-x}\text{Cd}_x\text{Te}$ Using Iterative Method

S. NAJAFI BAVANI AND M.S. AKHOUNDI KHEZRABAD\*

*Department of Physics, Payame Noor University (PNU), P.O. Box 19395-3697, Tehran, Iran*

Received: 29.04.2020 & Accepted: 21.12.2020

Doi: [10.12693/APhysPolA.139.97](https://doi.org/10.12693/APhysPolA.139.97)

\*e-mail: [ms\\_akhoundi@pnu.ac.ir](mailto:ms_akhoundi@pnu.ac.ir)

An iteration calculation was carried out to study electron transport properties in  $\text{Hg}_{1-x}\text{Cd}_x\text{Te}$ . We employed the modified iterative procedure so as to increase the computational accuracy in several structures. To calculate mobility, such mechanisms as deformation potential, polar optical phonon, piezoelectric, electron-hole and ionized impurity scattering were taken into consideration. The screening effects of the free carriers on scattering probabilities, band non-parabolicity, admixture of  $p$ -functions and arbitrary degeneracy of the electron distribution were considered. Electron drift mobility was calculated for different temperatures and doping dependences. The analysis suggested that the electron drift mobility decreases as the temperature increases from 100 K to 300 K. The temperature dependence of the MCT mobility results from the competition among various scattering mechanisms which are temperature-dependent. In the case of low temperatures (77 K), with increasing doping concentration, the electron mobility decreases quicker when compared to the high temperatures (150 and 300 K). Furthermore, we have concluded that the  $x$ -dependence of the  $\text{Hg}_{1-x}\text{Cd}_x\text{Te}$  mobility results primarily from the  $x$ -dependence of a bandgap as well as from the  $x$ -dependence of effective masses. Finally, it can be concluded that at  $p$ -type and intrinsic semiconductor ( $Z_x^T \leq 1$ ), the effect of the electron-hole scattering is significant while at  $n$ -type semiconductor ( $Z_x^T \gg 1$ ), the electron-hole scattering can be ignored.

topics: iteration method, electron drift mobility, scattering,  $\text{Hg}_{1-x}\text{Cd}_x\text{Te}$

## 1. Introduction

$\text{Hg}_{1-x}\text{Cd}_x\text{Te}$  (MCT) is a zinc-blende semiconductor mixed crystal, whose properties vary constantly with composition between their values in the constituent binary compounds. Because of its bandgap tunability with  $x$ ,  $\text{Hg}_{1-x}\text{Cd}_x\text{Te}$  has developed to become the most important material for detector applications over the entire IR range [1–4].  $\text{Hg}_{0.78}\text{Cd}_{0.22}\text{Te}$  and  $\text{Hg}_{0.7}\text{Cd}_{0.3}\text{Te}$  have been used for IR detection in 3–5 and 8–12  $\mu\text{m}$ . In order to design an electronic and optoelectronic device based on MCT, it is necessary to know the nature of transport carriers in them. The mobility [5] plays a central role in MCT devices since it determines a photoconductive gain in a photodetector [1], a dark current in a photovoltaic detector [6], and transport properties in a photoelectromagnetic detector (PEM) [7]. The mobility can be calculated theoretically from the solution of the Boltzmann transport equation. There are some numerical methods (i.e., the variation principle and iteration method) [8] and the Monte Carlo method [9]. The mobility of MCT has complex forms because of the band properties, including a small bandgap, small electron effective mass, large

non-parabolic conduction band, ionization energy, concentration of electron states and degree of compensation. Hence, the mobility of  $\text{Hg}_{1-x}\text{Cd}_x\text{Te}$  is dependent on  $x$  and temperature [1–9].

In this paper, using the iterative method, we calculate the low field drift mobility in  $\text{Hg}_{0.78}\text{Cd}_{0.22}\text{Te}$  and  $\text{Hg}_{0.7}\text{Cd}_{0.3}\text{Te}$ . Additionally, important scattering mechanisms such as polar-phonon, acoustic, piezoelectric, electron-hole, and ionized impurity scattering are considered.

This paper is organized as follows. Details of the iterative model and the electron mobility and scattering rates are presented in Sect. 2, the results of the iterative calculations carried out on  $\text{Hg}_{1-x}\text{Cd}_x\text{Te}$  structures are offered in Sect. 3 and conclusions are drawn in Sect. 4.

## 2. Theoretical model

The iterative technique is an approach to solve the Boltzmann transport equation (BTE) and to obtain the exact prediction of electron mobility in bulk semiconductors. We modified the Arabshahi iterative procedure [10] and this procedure allows us to increase the computational accuracy in several structures. The BTE describes how

the electron distribution function evolves under the action of a steady electric field  $\mathbf{E}$ . Hence, the BTE can be written as

$$\frac{e}{\hbar} \mathbf{E} \cdot \nabla f = \oint d\mathbf{k}' [s' f' (1 - f) - s f (1 - f')], \quad (1)$$

where  $f$  and  $s$  are the probability distribution functions and the differential scattering rates are  $f = f(\mathbf{k})$  and  $s = s(\mathbf{k}, \mathbf{k}')$ , respectively. The change from the equilibrium distribution function can be employed as a perturbation which is of first order in the electric field when the electric field is low. The distribution in the presence of a sufficiently low field can be assumed to be

$$f(\mathbf{k}) = f_0(|\mathbf{k}|) + g(|\mathbf{k}|) \cos(\theta), \quad (2)$$

where  $\theta$  is the angle between  $\mathbf{k}$  and  $\mathbf{E}$ . Next,  $f_0(|\mathbf{k}|) = f_0(k)$  and  $g(|\mathbf{k}|) = g(k)$  are the equilibrium distribution function and the isotropic function, respectively. They are proportional to the magnitude of the electric field, i.e.,

$$S(k, k') = S_{\text{el}}(k, k') + S_{\text{inel}}(k, k'). \quad (3)$$

The final elastic scattering rate  $S_{\text{el}}$  is the sum of the different scattering rates which are considered as elastic processes (acoustic, piezoelectric, electron-hole and ionized impurity scattering). The inelastic scattering rate  $S_{\text{inel}}$  is due to polar optical phonons. When the BTE is used and all differential scattering rates are considered, we can obtain the factor  $g(k)$  iteratively in the perturbed part of the distribution function  $f(\mathbf{k})$ . Namely,

$$\begin{aligned} g(k)[n] = & \left[ -\frac{e\mathbf{E}}{\hbar} \frac{\partial f_0}{\partial \mathbf{k}} + \sum_j \int g(k') [n-1] \right. \\ & \times \cos(\varphi) (S'_{\text{inel}j} (1-f) + S_{\text{inel}j} f) d\mathbf{k}' \\ & \times \left[ \sum_i \int (1 - \cos(\varphi)) S_{\text{el}i} d\mathbf{k}' \right. \\ & \left. \left. + \sum_j \int (S_{\text{inel}j} (1-f') + S'_{\text{inel}j} f') d\mathbf{k}' \right]^{-1}, \end{aligned} \quad (4)$$

where  $g(k)[n]$  is the perturbation to the distribution function after the  $n$ -th iteration, while the summations are over elastic  $i$  and inelastic  $j$  scattering processes. In the denominator the first term of integrand for the elastic scattering is the momentum relaxation rate. After the first iteration, the result of the relaxation time approximation can be achieved provided that the initial distribution is chosen to be the equilibrium distribution, for which  $g(k)$  is equal to 0. It becomes obvious that convergence for low electric fields can occur after only a few iterations. Once  $g(k)$  has been estimated to the required precision, then it is possible to compute such parameters as the drift mobility. The latter is given by

$$\mu_d = \frac{\hbar}{3m^*} \frac{\int_0^\infty k^3 g(k) \frac{1}{|\mathbf{E}|^d} dk}{\int_0^\infty k^2 f(\mathbf{k}) dk}, \quad (5)$$

with  $d$  defined as  $1/d = m^*(\nabla \mathbf{E})/(\hbar^2 k)$ , where  $\hbar$ ,  $k$  and  $m^*$  represent the reduced Planck constant, the wave electron vector and the effective

mass, respectively [10, 11]. In the following section, deformation potential, piezoelectric, polar optical phonon, ionized impurity and electron-hole scattering are analyzed.

### 2.1. Deformation potential scattering

Note that the acoustic modes adjust the interatomic spacing. Thus all, the location of the conduction and the valence band edges and the energy bandgap, differ with the location. Since the sensitivity of the band structure becomes related to the lattice spacing, the energy change of a band edge is determined by a deformation potential. The outcome of scattering of carriers is called the deformation potential scattering. The value of the energy domain of scattered acoustic phonons ranges from 0 to  $2\hbar\nu_s k$ , where  $\nu_s$  is the velocity of sound. The momentum conservation law limits the variation of phonon wave-vector to values from 0 to  $2k$ . The average amount of  $k$  is of the order of  $10^7 \text{ cm}^{-1}$  and the velocity of sound on average is of the order of  $10^7 \text{ cm/s}$ . Hence, the estimation  $2\hbar\nu_s k \sim 1 \text{ meV}$  turns out not substantial when it is compared to the thermal energy at room temperature. As a result, the deformation potential scattering of acoustic modes can be considered as an elastic process (except for very low temperatures). The deformation-potential scattering rate with either phonon emission or absorption for an electron of energy  $\epsilon$  is defined applying the Fermi's golden rule accordingly

$$\begin{aligned} P_{\text{ab}}(\epsilon) = & \frac{\sqrt{2(m^*)^3} D_{\text{ac}}^2 k_{\text{B}} T}{\pi \rho \nu^2 \hbar^3} \frac{\sqrt{\epsilon(1+\alpha\epsilon)}}{(1+2\alpha\epsilon)} \\ & \times \left( (1+\alpha\epsilon)^2 + \frac{1}{3} \alpha^2 \epsilon^2 \right). \end{aligned} \quad (6)$$

Here,  $D_{\text{ac}}$ ,  $k_{\text{B}}$ ,  $\rho$ ,  $\alpha$  and  $T$  are the acoustic deformation potential, the Boltzmann constant, the material density, the nonparabolicity coefficient of the conduction band, and the lattice temperature, respectively. This formula clearly shows that the acoustic scattering increases with the increasing temperature [12, 13].

### 2.2. Piezoelectric scattering

The later type of electron scattering by acoustic modes happens when the displacements of the atoms build an electric field through the piezoelectric effect. This can happen in the compound semiconductors such as the II-VI and III-V materials and include  $\text{Hg}_{1-x}\text{Cd}_x\text{Te}$  which in fact has a relatively large piezoelectric constant.

Ridley considered the piezoelectric scattering rate for an electron of energy  $\epsilon$  as

$$\begin{aligned} P_{\text{pz}}(\epsilon) = & \frac{1}{4\sqrt{2}\pi} \frac{\sqrt{m^*} e^2 K_{\text{ac}}^2 k_{\text{B}} T}{\epsilon_0 \epsilon_s \hbar^2} \frac{(1+2\alpha\epsilon)^2}{\sqrt{\gamma(E)}} \\ & \times \left[ \ln \left( 1 + \frac{8m^* \gamma(\epsilon)}{\hbar^2 q_0^2} \right) - \frac{1}{1 + \hbar^2 q_0^2 / (8m^* \gamma(\epsilon))} \right. \\ & \left. + \frac{(2\alpha\epsilon)^2}{2(1+2\alpha\epsilon)^2} \right], \end{aligned} \quad (7)$$

where  $K_{ac}$ ,  $\epsilon_0$ , and  $\epsilon_s$  are the average electromechanical coupling constant, the vacuum permittivity constant and the relative dielectric constant of the material, respectively. Note that they are dimensionless. We use an energy-wave vector relation of the type

$$\gamma(\epsilon) = \epsilon(1 + \alpha\epsilon) = \frac{\hbar^2 k^2}{2m^*}, \quad (8)$$

with

$$\alpha = \frac{1}{\epsilon_g} \left(1 - \frac{m^*}{m_0}\right)^2, \quad (9)$$

where  $\epsilon_g$  is the bandgap of the material and  $m_0$  is the mass of free electrons [14].

### 2.3. Polar optical phonon scattering (POP)

The dipolar electric field arising from the contrary displacement of the negatively and positively charged atoms makes a coupling between the electrons and the lattice which results in electron scattering. As a result of this process, the scattering rate for an electron of energy  $\epsilon$  is

$$R_{po}(\epsilon) = \frac{e^2 \sqrt{2m^*} \omega_{op}}{8\pi\epsilon_0 \hbar} \left( \frac{1}{\epsilon_\infty} - \frac{1}{\epsilon_s} \right) \times \frac{1 + 2\alpha\epsilon'}{\sqrt{\gamma(\epsilon)}} F_0(\epsilon, \epsilon') \{N_{op}, N_{op} + 1\}, \quad (10)$$

where  $N_{op}$  is the phonon occupation number and  $\hbar\omega_{op}$  is the polar optical phonon energy [12–14]. Now,

$$\epsilon' = \begin{cases} \epsilon + \hbar\omega_{op} & (\text{absorption}), \\ \epsilon - \hbar\omega_{op} & (\text{emission}), \end{cases} \quad (11)$$

is the final energy state in a phonon absorption (upper case) and a phonon emission process (lower case). The other quantities are read as

$$F_0(\epsilon, \epsilon') = \frac{1}{C} \left[ A \ln \left| \frac{\sqrt{\gamma(\epsilon)} + \sqrt{\gamma(\epsilon')}}{\sqrt{\gamma(\epsilon)} - \sqrt{\gamma(\epsilon')}} \right| + B \right],$$

$$A = \left[ 2(1 + \alpha\epsilon)(1 + \alpha\epsilon') + \alpha(\gamma + \gamma') \right]^2,$$

$$B = -2\alpha\sqrt{\gamma\gamma'} [4(1 + \alpha\epsilon)(1 + \alpha\epsilon') + \alpha(\gamma + \gamma')],$$

$$C = 4(1 + \alpha\epsilon)(1 + \alpha\epsilon')(1 + 2\alpha\epsilon)(1 + 2\alpha\epsilon'). \quad (12)$$

### 2.4. Intravalley impurity scattering

The Brook–Herring (BH) technique [15] is the standard method for dealing with ionized impurity scattering in semiconductors. The differential scattering rate for ionized impurity can be written by the BH technique as

$$P_{ii}(\epsilon) = \frac{8\pi e^4 \sqrt{(m^*)^3}}{\epsilon_s^2 \hbar q_0} N_d \sqrt{\gamma(\epsilon)} + \frac{1 + 2\alpha\epsilon}{1 + 4\sqrt{2m^*} \hbar q_0 \gamma(\epsilon)}, \quad (13)$$

where  $q_0$  and  $N_d$  are the inverse screening length and the donor concentration, respectively [13].

### 2.5. Electron–hole scattering

According to [16–18], the electron–hole scattering rate can be calculated similarly to the rate of electron scattering on charged impurities when the effective mass of the hole is much heavier than that of the electron. The electron–hole scattering rate is given by (12), where the concentration of charged impurities should be replaced by the effective number of holes. For the electron–hole scattering, both the screening function and the effective number of holes strongly depend on the position of the Fermi level. In this work, the electron–hole scattering was considered as an elastic mechanism.

The main scattering parameters used in this method are reported in Table I [19, 20].

## 3. Results and discussion

In this situation, we introduce normalized doping concentration

$$Z_x^T = \frac{N_d}{n_i(x, T)} \quad (14)$$

being a function of temperature  $T$  and  $x$ . Here,  $N_d$  is the donor concentration,  $n_i(x, T)$  is the intrinsic concentration and  $Z_x^T$  is the measure for the doping regime. It should be mentioned that for  $n$ -type semiconductor,  $Z_x^T$  is greater than one.

Figure 1 shows the energy dependence of individual and total scattering rates in  $\text{Hg}_{1-x}\text{Cd}_x\text{Te}$  for  $x = 0.22$  and  $0.3$ . Here, the donor concentration is taken to be  $N_d = 10^{17} \text{ cm}^{-3}$  ( $Z_{0.22}^{300\text{K}} = 10$ ) for  $x = 0.22$  and  $N_d = 10^{16} \text{ cm}^{-3}$  ( $Z_{0.3}^{300\text{K}} = 10$ ) for  $x = 0.3$  at 300 K. As depicted in Fig. 1, the ionized impurity scattering is dominant in the case of low-energy but then the polar optical phonon (emission) scattering becomes dominant in more energies. Thus, the marked reduction in mobility can be ascribed to the polar optical phonon (emission) scattering.

TABLE I

Parameters of  $\text{HgCdTe}$ , as used in the iterative method [19, 20].

Notation	Unit	$x$ (composition in Cd)		
		0.22	0.3	Ref.
$\nu$	$[\text{ms}^{-1}]$	2054	2077	[19]
$\rho$	$[\text{kg}/\text{m}^3]$	7544	7360	[19]
$\epsilon_0$	–	17.34	16.33	[19]
$\epsilon_\infty$	–	12.16	11.25	[19]
$D_{ac}$	$[\text{eV}]$	9.47	9.45	[20]
$\omega_{op}$	$[\text{eV}]$	0.0183	0.0184	[20]
$a$	$[\text{Å}]$	6.4640	6.4653	[19, 20]
$p$	$[\text{C}/\text{cm}^2]$	0.028	0.029	[20]
$\alpha$	$[\text{eV}^{-1}]$	5.3515	3.2992	calc.
$\epsilon_g$	$[\text{eV}]$	0.1819	0.2906	[19, 20]
$m^*$	–	0.0134	0.0209	[20]

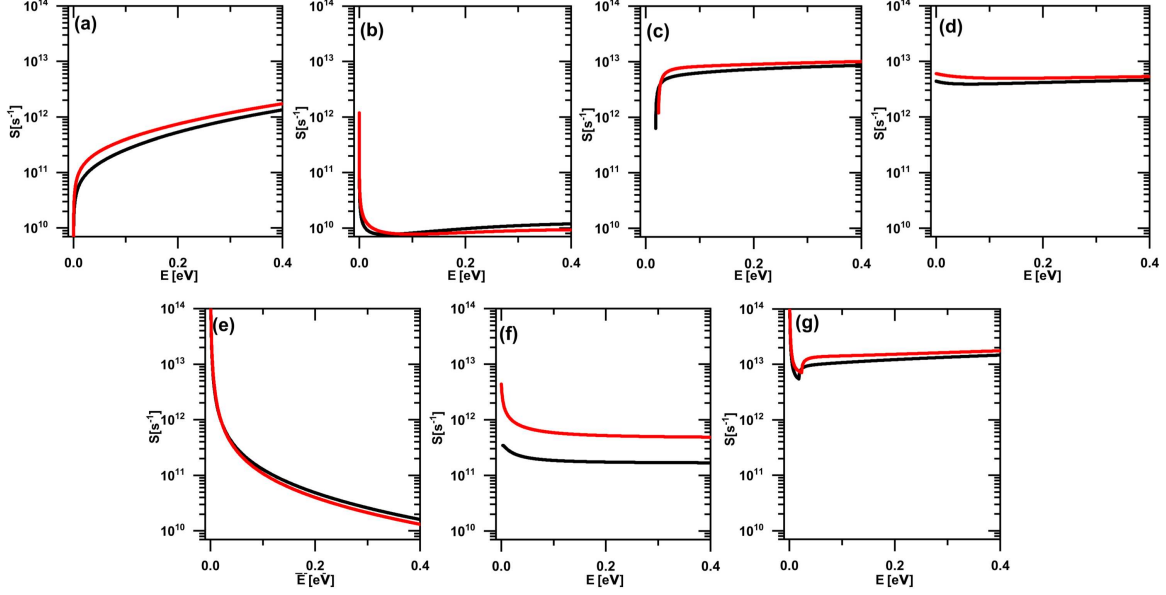


Fig. 1. Calculated electron scattering rates as a function of energy for bulk  $\text{Hg}_{0.78}\text{Cd}_{0.22}\text{Te}$  (black line) and  $\text{Hg}_{0.7}\text{Cd}_{0.3}\text{Te}$  (red line) at  $T = 300$  K and the donor concentration is taken to be  $N_d = 10^{17} \text{ cm}^{-3}$  for  $x = 0.22$  and  $N_d = 10^{16} \text{ cm}^{-3}$  for  $x = 0.3$ : (a) acoustic phonon, (b) piezoelectric, (c) polar-optical phonon (emission), (d) polar-optical phonon (absorption), (e) ionized impurity, (f) electron-hole, (g) total scattering rate.

The electron mobility versus temperature for bulk  $\text{Hg}_{0.78}\text{Cd}_{0.22}\text{Te}$  and  $\text{Hg}_{0.7}\text{Cd}_{0.3}\text{Te}$  are shown in Fig. 2. The electron drift mobility decreases with the increasing temperature due to the increasing optical phonon scattering rate. Also, we can observe a maximum in the mobility versus temperature at temperatures 50 K and 65 K for  $\text{Hg}_{0.78}\text{Cd}_{0.22}\text{Te}$  and  $\text{Hg}_{0.7}\text{Cd}_{0.3}\text{Te}$ , respectively. This is because at high temperatures ( $T > 50$  K), the mobility is dominated by lattice scattering mechanisms, which obey the empirical functional form of  $T^{-3/2}$ , and at low temperatures ( $T < 50$  K), the mobility begins to be dominated by the impurity scattering mechanism, which obeys the empirical function form of  $T^m$  (where  $m$  is usually between 0 and 1.5). Given the fact that the intrinsic concentration of HgCdTe is a function of temperature, we have  $Z_x^T \gg 1$  at  $T < 300$  K. Nonetheless, when  $T > 300$  K and  $Z_x^T$  becomes virtually one, HgCdTe becomes intrinsic. As a result, the hole concentration settles near the donor concentration  $N_d = 10^{17} \text{ cm}^{-3}$  and makes the electron-hole scattering rate increase and eventually also makes the mobility decrease. Therefore, it can be concluded that when the mobility curve versus the temperature is concerned, if  $Z_x^T$  is smaller or closer to one, the mobility decreases due to electron-hole scattering and when  $Z_x^T$  is greater than one, it has no effect on the amount of mobility and can be ignored.

The competition between different scattering mechanisms in the case of  $x = 0.3$  is not serious when compared to the case of  $x = 0.2$ . This is because its slope of the curve is less than  $x = 0.22$  and it is due to the difference between their band structure and effective mass.

Figure 3 shows the variation of the electron mobility as a function of donor concentration. HgCdTe is an  $n$ -type semiconductor in the doping range  $10^{14} \text{ cm}^{-3}$  up to  $10^{18} \text{ cm}^{-3}$  at 77 K by considering the intrinsic concentration  $n_i(0.22, 77) = 10^{13} \text{ cm}^{-3}$  and  $n_i(0.3, 77) = 10^9 \text{ cm}^{-3}$ . Its mobility decreases as the donor concentration increases since the ionized impurity scattering rate increases. Figure 3a shows that the curves of 150 K and 300 K behave differently from the curve of 77 K at  $Z_x^T < 1$  when the donor concentration is less than  $n_i(0.22, 150) = 10^{15}$  and  $n_i(0.22, 300) = 10^{16}$ . Therefore, the hole concentration increases in this range and the electron-hole scattering rate increases too, leading to mobility reduction. Similar behavior is observable for  $x = 0.3$ . It can be

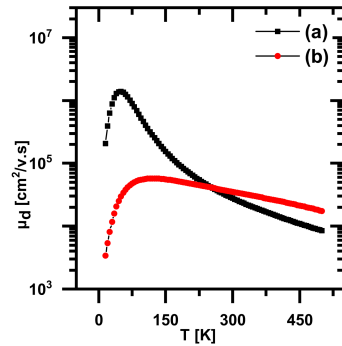


Fig. 2. The electron mobility versus temperature for bulk  $\text{Hg}_{0.78}\text{Cd}_{0.22}\text{Te}$  (a) and  $\text{Hg}_{0.7}\text{Cd}_{0.3}\text{Te}$  (b) from 10 K to 500 K and the donor concentration is taken to be  $N_d = 10^{17} \text{ cm}^{-3}$  for  $x = 0.22$  and  $N_d = 10^{16} \text{ cm}^{-3}$  for  $x = 0.3$ .

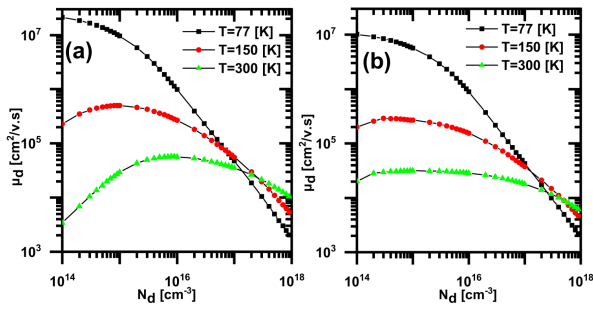


Fig. 3. Variations of electron mobility in terms of concentration in  $T = 77, 150,$  and  $300$  K for (a)  $\text{Hg}_{0.78}\text{Cd}_{0.22}\text{Te}$ , (b)  $\text{Hg}_{0.7}\text{Cd}_{0.3}\text{Te}$ .

concluded that for the donor concentration that leads to  $Z_x^T$ , which is less than or equal to one, the effect of electron–hole scattering is significant and for  $Z_x^T$ , which is much larger than one, the electron–hole scattering can be ignored (as shown in Figs. 2 and 3).

#### 4. Conclusions

The main conclusion that can be drawn from this research is that the electron mobility was obtained for zinc-blende  $\text{Hg}_{1-x}\text{Cd}_x\text{Te}$  structures. This study used the iterative method in the low applied field and such scattering mechanisms as deformation potential, polar optical phonon, piezoelectric, electron–hole and ionized impurity scattering were considered. Figure 1 shows that all scattering rates are dependent on  $x$  because of the bandgap dependence of  $x$  excepting ionized impurity and piezoelectric scattering rates. Also, the polar optical phonon (emission) scattering is dominant in the energy range of  $0.05\text{--}0.4$  eV at room temperature and low electric field. As evident from Fig. 2, the variation of the mobility — as a function of temperature — indicates how different scattering mechanisms compete with one another at different temperature ranges. Due to impurity and the polar optical phonon (emission) scattering characteristics, the mobility shows its maximum at about  $50$  K. However, the slope in Fig. 2b is less than that in Fig. 2a since there is a competition between different scattering mechanisms.

The analysis also suggested the low-field electron mobility is higher for  $\text{Hg}_{1-x}\text{Cd}_x\text{Te}$  structures with lower  $x$  primarily because of the  $x$ -dependence of a bandgap, as well as the  $x$ -dependence of effective masses. From the analysis of Figs. 2 and 3, this can also be concluded that the effect of electron–hole scattering is significant at  $Z_x^T \leq 1$  and can be neglected at  $Z_x^T \gg 1$ .

It is worth to remember that  $Z_x^T$  is a simple criterion for the interpretation of the dependent simultaneous mobility to doping and temperature.

#### References

- [1] M. Strojnik, M. D’Acunto, A. Rogalski, *Appl. Opt.* **57**, AITA1 (2018).
- [2] A. Rogalski, M. Kopytko, P. Martyniuk, *Appl. Opt.* **57**, D11 (2018).
- [3] J. Rothman, *J. Electron. Mater.* **47**, 5657 (2018).
- [4] I.I. Izhnin, K.D. Mynbaev, A.V. Voitsekhevskii et al., *Semicond. Sci. Technol.* **35**, 115019 (2020).
- [5] S. Poncé, W. Li, S. Reichardt, F. Giustino, *Rep. Prog. Phys.* **83**, 036501 (2020).
- [6] B. Barutcu, Ph.D. Thesis, Middle East Technical University, 2019.
- [7] A.G. Korotaev, I.I. Izhnin, K.D. Mynbaev, et al., *Surf. Coat. Technol.* **393**, 125721 (2020).
- [8] E.O. Melezhik, J.V. Gumenjuk-Sichevska, F.F. Sizov, *Springerplus* **5**, 80 (2016).
- [9] S. Derelle, S. Bernhardt, R. Haïdar, J. Primot, J. Deschamps, J. Rothman, *IEEE Trans. Electron. Dev.* **56**, 569 (2009).
- [10] H. Arabshahi, A.A. Mowlavi, *Mod. Phys. Lett. B* **23**, 1359 (2009).
- [11] D.L. Rode, in: *Semiconductors and Semimetals*, Vol. 10, Eds. R.K. Willardson, A.C. Beer, Academic Press, New York 1975, p. 1.
- [12] C. Jacoboni, *Theory of Electron Transport in Semiconductors: A Pathway from Elementary Physics to Nonequilibrium Green Functions*, Vol. 165, Eds. M. Cardona, P. Fulde, K. von Klitzing, R. Merlin, H.-J. Queisser, H. Störmer, Springer Sci.+Busin. Media, Heidelberg 2010.
- [13] K. Seeger, *Semiconductor Physics*, Springer Sci.+Busin. Media, 2013.
- [14] J. Chu, A. Sher, in: *Physics and Properties of Narrow Gap Semiconductors*, Springer Sci.+Busin. Media, New York 2008.
- [15] H. Brooks, C. Herring, *Phys. Rev.* **83**, 879 (1951).
- [16] S.D. Yoo, K.D. Kwack, *J. Appl. Phys.* **81**, 719 (1997).
- [17] W. Szymańska, T. Dietl, *J. Phys. Chem. Solids* **39**, 1025 (1978).
- [18] E.O. Melezhik, J.V. Gumenjuk-Sichevska, F.F. Sizov, *J. Appl. Phys.* **118**, 194305 (2015).
- [19] R.D.S. Yadava, A.K. Gupta, A.V.R. Warrior, *J. Electron. Mater.* **23**, 1359 (1994).
- [20] K.F. Brennan, N.S. Mansour, *J. Appl. Phys.* **69**, 7844 (1991).